Numerical analyses on optical limiting performances of chloroindium phthalocyanines with different substituent positions*

Yu-Jin Zhang(张玉瑾)[1], Xing-Zhe Li(李兴哲)[2], Ji-Cai Liu(刘纪彩)[2], and Chuan-Kui Wang(王传奎)[1,†]

[1] College of Physics and Electronics, Shandong Normal University, Jinan 250014, China
[2] Mathematics and Physics Department, North China Electric Power University, Beijing 102206, China

(Received 29 July 2015; revised manuscript received 21 August 2015; published online 1 December 2015)

Optical limiting properties of two soluble chloroindium phthalocyanines with α- and β-alkoxyl substituents in nanosecond laser field have been studied by solving numerically the coupled singlet–triplet rate equation together with the paraxial wave field equation under the Crank–Nicholson scheme. Both transverse and longitudinal effects of the laser field on photophysical properties of the compounds are considered. Effective transfer time between the ground state and the lowest triplet state is defined in reformulated rate equations to characterize dynamics of singlet–triplet state population transfer. It is found that both phthalocyanines exhibit good nonlinear optical absorption abilities, while the compound with α-substituent shows enhanced optical limiting performance. Our *ab-initio* calculations reveal that the phthalocyanine with α-substituent has more obvious electron delocalization and lower frontier orbital transfer energies, which are responsible for its preferable photophysical properties.

Keywords: optical limiting, nanosecond laser field, phthalocyanine

PACS: 33.80.–b, 82.50.Pt, 31.15.A– **DOI:** 10.1088/1674-1056/25/1/013302

1. Introduction

Materials exhibiting significant nonlinear optical effects have drawn wide attention on account of their potential applied value as optical limiters in protection of eyes and optical sensors against intense light.[1–4] Reverse saturable absorption (RSA) is an especially effective mechanism in producing large nonlinear absorption.[5–8] This mechanism requires two criteria. First, the material must have a larger excited state absorption (ESA) cross section than the ground-state absorption (GSA) cross section. Second, the lifetime of the excited state must be long enough.[9] A variety of organometallic and organic materials have been found to fulfill these criteria, among which phthalocyanines (Pcs) with large delocalized π-conjugated electron systems are promising candidates because of their extraordinary mechanical properties, environmental stability, and ease of process ability.[10–12]

However, most of the Pcs are easy to aggregate and show poor solubility in common solvents because of strong interactions among molecules, which is not conducive to their application.[13,14] Fortunately, Pcs' solubility can be effectively improved by introducing substituted groups.[15] Different kinds and positions of the substituents may cause different effects on their physicochemical performances.[16,17] Nyokong *et al*. provided a review focusing on the photochemical and photophysical properties of metallophthalocyanine complexes containing main group metals and some unmetallated phthalocyanine complexes.[17] Snow *et al*. synthesized a series of methyl-terminated oligooxyethylene-substituted phthalocyanines with different peripheral substitutions, indicating that both tetra-α- and tetra-β-substituted compounds were reverse saturable absorbers in the visible region of the spectrum, but the former had larger nonlinear absorption coefficient and could be a useful optical limiter.[18]

Recently, Wang *et al*. synthesized two soluble heavy-metal phthalocyanine derivatives, namely, tetra-α-(2-ethylbutoxy) chloroindium phthalocyanine (α-InPcCl) and tetra-β-(2-ethylbutoxy) chloroindium phthalocyanine (β-InPcCl), and studied their optical limiting (OL) behaviors in THF solution with a 532-nm nanosecond laser. It was found that α-InPcCl was superior to β-InPcCl as OL material.[19] To give an insight into the physical mechanism, we theoretically investigate the photophysical properties of these two phthalocyanines in this paper. The dynamics of pulse propagation and photoabsorption are studied by solving numerically the coupled rate equations and paraxial wave equations. Rate equations for the generally used five-level model are reformulated into one equivalent rate equation according to the time hierarchies of the studied systems.[20] Paraxial wave equation together with the rate equation is solved in the local time frame by use of Crank–Nicholson numerical method. Our simulation results are in good agreement with the experimental measurements in Ref. [19]. *Ab-initio* calculations on the electronic structures of these compounds indicate that α-InPcCl has extended electron delocalization and lower frontier orbital

*Project supported by the National Basic Research Program of China (Grant No. 2011CB808100), the National Natural Science Foundation of China (Grant Nos. 11204078 and 11574082), and the Fundamental Research Funds for the Central Universities of China (Grant No. 2015MS54).

†Corresponding author. E-mail: ckwang@sdnu.edu.cn

© 2016 Chinese Physical Society and IOP Publishing Ltd

transfer energies, which means that α-InPcCl can be more efficiently excited in photophysical processes and possesses better OL properties than β-InPcCl.

2. Outline of theoretical methods

We simplify the transition scheme as a generalized five-level model (Fig. 1) when considering the interaction between the molecule and the optical laser field. This scheme takes into account two sequential two-photon absorption (TPA) channels: $(S_0 \to S_1) \times (S_1 \to S_n)$ and $(S_0 \to S_1) \times (T_1 \to T_2)$. Here the coherent one-step TPA and one-photon transition $S_0 \to S_n$ are ignored because the frequency of the light is tuned around the resonance frequency of the one-photon transitions between two adjacent states $(S_0 \to S_1)$, $(S_1 \to S_n)$, and $(T_1 \to T_2)$.

2.1. Rate equations in nanosecond time domain

Rate equations for populations of the singlet and triplet states involved in the studied processes can be written as follows:

$$\begin{aligned}
&\frac{\partial}{\partial t}\rho_{S_0} = -\gamma(t)(\rho_{S_0}-\rho_{S_1}) + \Gamma_{S_1}\rho_{S_1} + \Gamma_{T_1}\rho_{T_1},\\
&\left(\frac{\partial}{\partial t} + \Gamma_{S_1} + \gamma_{\rm c}\right)\rho_{S_1}\\
&= \Gamma_{S_n}\rho_{S_n} - \gamma_S(t)(\rho_{S_1}-\rho_{S_n}) + \gamma(t)(\rho_{S_0}-\rho_{S_1}),\\
&\left(\frac{\partial}{\partial t} + \Gamma_{S_n}\right)\rho_{S_n} = \gamma_S(t)(\rho_{S_1}-\rho_{S_n}),\\
&\left(\frac{\partial}{\partial t} + \Gamma_{T_2}\right)\rho_{T_2} = \gamma_T(t)(\rho_{T_1}-\rho_{T_2}),
\end{aligned} \tag{1}$$

where $\gamma(t)$, $\gamma_S(t)$, and $\gamma_T(t)$ are respectively the field-induced rates of one-photon transitions $S_0 \to S_1$, $S_1 \to S_n$, and $T_1 \to T_2$. The $\gamma_{\rm c}$ is the rate of intersystem crossing transition $S_1 \to T_1$. Γ_{S_1}, Γ_{S_n}, Γ_{T_1}, and Γ_{T_2} are the decay rates of the states S_1, S_n, T_1, and T_2, respectively. Rate equation for the population of the state T_1 is not given in Eq. (1) because the population ρ_{T_1} can be got through the particle conservation law $\sum_k \rho_k = 1$.

It is convenient to express the one-photon induced transition $(m \to n)$ rate through the corresponding transition dipole moments d_{mn} or the photon absorption cross sections σ_{mn}[21]

$$\gamma_{mn}(t) = \frac{|d_{mn}|^2 I(t)}{3\hbar^2 c\varepsilon_0}\frac{\Gamma_{mn}}{\Omega_{mn}^2+\Gamma_{mn}^2} = \frac{\sigma_{mn}I(t)}{\hbar\omega}\frac{\Gamma_{mn}}{\Omega_{mn}^2+\Gamma_{mn}^2}, \tag{2}$$

where $I(t)$ is the intensity of the field, $I = c\varepsilon_0|E|^2/2$, and $\Omega_{mn} = \omega - \omega_{mn}$ is the detuning of the light frequency ω from the resonant frequency ω_{mn}. Γ_{mn} is determined by the sum of the lifetime broadenings of the two levels and the inhomogeneous broadenings. In solutions, inhomogeneous broadenings are the largest ones, so Γ_{mn} is set to be the same value of $\hbar\Gamma_{mn} = \hbar\Gamma = 0.1$ eV for all transitions.

For the studied system, Γ_{S_n}, Γ_{T_2} are of the magnitude of ps^{-1}, $\gamma_{\rm c}$ and Γ_{T_1} are of the magnitude of ps^{-1}–ns^{-1} and μs^{-1}, respectively, while the laser pulse stays of the ns magnitude. Due to the different timescales of the system, numerical simulation will be time-consuming. However, one can divide the system into fast subsystem (S_1, S_n, T_2) and slow subsystem (S_0, T_1) under the condition[20,22]

$$\begin{aligned}
&\tau,\ \tau_{\rm ST} \gg (\Gamma_{S_1} + \gamma_{\rm c} + \gamma(t) + \gamma_S(t))^{-1},\\
&(\Gamma_{S_n} + \gamma_S(t))^{-1},\ (\Gamma_{T_2} + \gamma_T(t))^{-1}.
\end{aligned} \tag{3}$$

Here τ is the pulse duration and $\tau_{\rm ST}$ is the effective population transfer time from the ground state S_0 to the lowest triplet state T_1.

The condition (3) indicates that populations of the excited states follow adiabatically the slow dynamics of S_0 and T_1 states. Thus one can mathematically disregard the time derivatives in Eq. (1) except for the equation of the ground state population and lowest triplet state population. Finally one can obtain the following single time-dependent equation for the ground state instead of the rate equations (1) to describe the population dynamics of the multilevel molecules:

$$\frac{\partial}{\partial t}\rho_{S_0} = -\gamma_0(t)\rho_{S_0} + \Gamma_{T_1}P(t) = \frac{q(t)-\rho_{S_0}}{\tau_{\rm ST}(t)}, \tag{4}$$

where $q(t) = \tau_{\rm ST}(t)\Gamma_{T_1}P(t)$, $\tau_{\rm ST}(t) = 1/\gamma_0(t)$, $\gamma_0(t) = \gamma(t)\Phi(t) + \Gamma_{T_1}Q(t)$, $\Phi(t) = \gamma_{\rm c}/(\Gamma_{S_1}+\gamma_{\rm c}+\gamma(t))$, $P(t) = 1/(1+w_{T_2}(t))$, and $Q(t) = P(t)[1+w(t)(1+w_S(t))]$.

Auxiliary quantities $w(t)$, $w_S(t)$, $w_{T_2}(t)$ have physical meanings of relative probabilities for radiative one-photon transitions $S_1 \to S_0$, $S_n \to S_1$, and $T_2 \to T_1$, respectively,[20]

$$\begin{aligned}
&w(t) = \frac{\gamma(t)}{\Gamma_{S_1}+\gamma_{\rm c}+\gamma(t)},\quad w_S(t) = \frac{\gamma_S(t)}{\Gamma_{S_n}+\gamma_S(t)},\\
&w_{T_2}(t) = \frac{\gamma_T(t)}{\Gamma_{T_2}+\gamma_T(t)}.
\end{aligned} \tag{5}$$

2.2. Paraxial wave equation

Considering the incident laser field

$$\varepsilon(\boldsymbol{r},t) = \boldsymbol{E}(\boldsymbol{r},t)\cos(\boldsymbol{k}\cdot\boldsymbol{r} - \omega t), \tag{6}$$

Maxwell's equations can be reduced to the well-known paraxial wave equation within the slowly varying envelope approximation (SVEA), which can be reformed through the photon absorption cross section as follows:

$$\left(\frac{\partial}{\partial z} + \frac{n_0}{c}\frac{\partial}{\partial t} - \frac{\mathrm{i}}{2k}\Delta_\perp\right)\boldsymbol{E} = -\left(\frac{N\sigma_{\rm tot}}{2} - \mathrm{i}k\frac{\delta n}{n_0}\right)\boldsymbol{E}, \tag{7}$$

where $\Delta_\perp$ is the transverse Laplace operator, which can be written as

$$\Delta_\perp = \frac{\partial^2}{\partial r^2} + \frac{1}{r}\frac{\partial}{\partial r} + \frac{1}{r^2}\frac{\partial^2}{\partial\phi^2}$$

in cylindrical coordinates, $k = n_0\omega/c$, n_0 is the equilibrium refraction index, δn is the light-induced deviation of the refraction index from the equilibrium value n_0, and $\sigma_{\rm tot}$ is the

total photoabsorption cross section and given by

$$\sigma_{\rm tot} = \sigma_{S_1S_0}(\rho_{S_0}-\rho_{S_1})+\sigma_{S_nS_1}(\rho_{S_1}-\rho_{S_n}) + \sigma_{T_2T_1}(\rho_{T_1}-\rho_{T_2}). \quad (8)$$

2.3. Calculation details

The incident laser field is isotropic in the transverse direction and has a form of a Gaussian beam

$$\begin{aligned} \boldsymbol{E}(r,z,T) &= \varepsilon_0(T)\frac{w_0}{w(z)}\exp\left(-\frac{r^2}{w^2(z)}\right) \\ &\quad\times\exp\left(\mathrm{i}k\frac{r^2}{2R(z)}-\mathrm{i}\zeta(z)\right), \\ R(z) &= z\left[1+\left(\frac{l_0}{z}\right)^2\right], \quad \zeta(z)=\arctan\left(\frac{z}{l_0}\right), \\ w(z) &= w_0\sqrt{1+(z/l_0)^2}, \\ T_0 &= t-n_0z_0/c, \quad l_0=\pi w_0^2/\lambda, \end{aligned} \quad (9)$$

where $T = t - n_0 z/c$ is the retarded time, l_0 is the Rayleigh length, $w(z)$ is the beam width, $R(z)$ is the radius of the Gaussian spherical wave, and $\zeta(z)$ is the Gouy phase. In simulations, paraxial equation (7) is solved with the boundary conditions $r\boldsymbol{E}(r,z,T)=0$ for $r=0,\ 5w(z)$.

The temporal shape of the initial pulse is also modeled by a Gaussian shape

$$\varepsilon_0(t) = \varepsilon_0\,\mathrm{e}^{-1/2((t-t_0)/\tau)^2\ln 2}, \quad (10)$$

where τ is the half width at half maximum (HWHM). In the present work, simulations are performed for $\tau = 7.0$ ns, $t_0 = 2.5\tau$, $w_0 = 1$ mm, and $n_0 \approx 1$. Considering that the focal point of the Gaussian pulse and the center of the medium are both localized at $z = 0$, the entry of the pulse is at $z_0 = -L/2$, where L is the length of absorbing cell.

The studied molecular structures of α-InPcCl and β-InPcCl, as well as the scheme of transitions, are presented in Fig. 1. To perform numerical simulations, relaxation rates and resonant transition energies as well as one-photon absorption cross sections ($\lambda = 532$ nm) of these compounds are extracted from the experiments (see Table 1).[19] Lifetimes of excited states (S_n, T_2) which usually lie in the picosecond region are assumed to be $1/\Gamma_{S_n} = 1/\Gamma_{T_2} = 1$ ps. The one-photon transition cross section $\sigma_{S_1S_n}$ is set to be 1.0×10^{-21} m^2.[22] In order to save computational time, the simulations are performed for relatively high concentrations and short propagation distances compared with experimental parameters using the scaling relation $N_{\rm cal}L_{\rm cal} = N_{\rm exp}L_{\rm exp}$ ($L_{\rm cal} = 0.8$ mm, $L_{\rm exp} = 1.0$ cm).

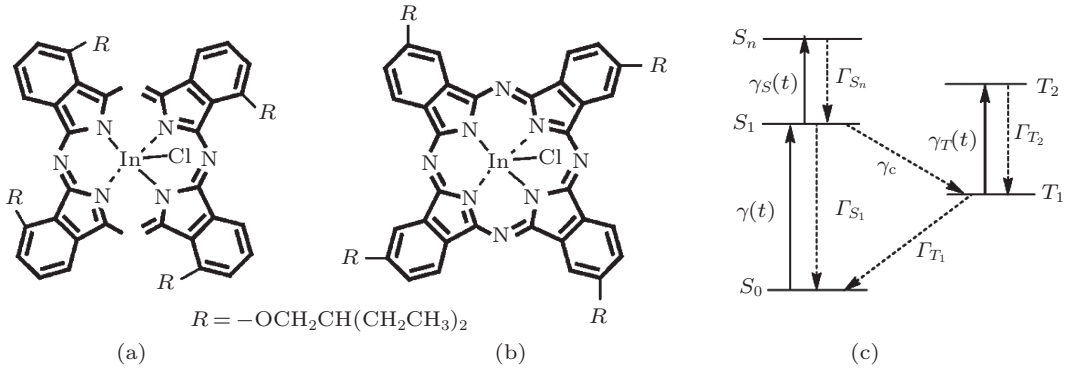


Fig. 1. Structures of (a) α-InPcCl, (b) β-InPcCl, and (c) the scheme of transitions.

Table 1. Photophysical parameters of α-InPcCl and β-InPcCl.[19]

Mol.	$E_{S_0S_1}$/eV	$E_{T_1T_2}$/eV	$\gamma_c/10^8$ s^{-1}	τ_{T_1}/μs	$\sigma_{S_0S_1}/10^{-18}$ cm^2	$\sigma_{T_1T_2}/\sigma_{S_0S_1}$	$N_{\rm cal}/10^{24}$ m^{-3}
α-InPcCl	1.71	2.12	11.2	18.0	1.37	23.7	1.30
β-InPcCl	1.77	2.48	1.19	28.6	10.0	11.3	0.31

Ab-initio calculations for α-InPcCl and β-InPcCl are performed as follows. Time-dependent DFT/B3LYP method implemented in Gaussian09 package[23] is employed to obtain the optimized geometric and electronic structures. 6-31G* and Lanl2dz basis sets are chosen for light atoms and heavy-metal indium (In) atom, respectively. Frontier orbitals and charge density differences between charge transfer (CT) states and ground states are visualized for understanding the mechanism of the photophysical properties of the molecules.

3. Results and discussion

It can be seen from Eq. (4) that dynamics of the population is mainly defined by the effective transfer time $\tau_{\rm ST}$ between the ground state S_0 and the lowest triplet state T_1, which depends crucially on the intensity of pulse. Figure 2 shows this characteristic time without taking into account the propagation effect. Due to the Gaussian distribution of the pulse, the central part with higher intensity leads to shorter population

transfer time. Moreover, influence of the substituent position on the population transfer process is shown. At the same level of the field intensity, population transfer rate from the ground state S_0 to the triplet state T_1 for α-InPcCl is always faster than that for β-InPcCl on account of the larger intersystem crossing rate γ_c of α-InPcCl, indicating that α-InPcCl has better nonlinear optical properties.

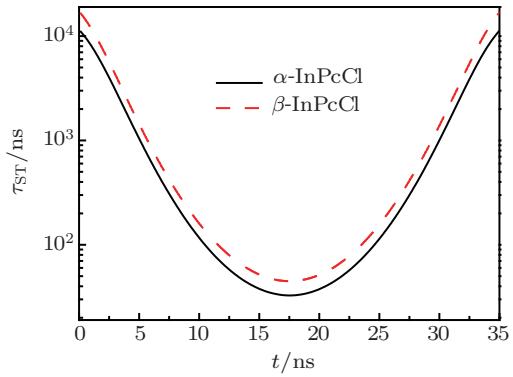


Fig. 2. (color online) Response time of population transfer between the singlet and the triplet states $S_0 \rightarrow T_1$ for α-InPcCl (solid line) and β-InPcCl (dashed line) without propagation of the pulse ($z = 0$). $I_0 = 4 \times 10^{12}$ W/m^2.

In order to investigate the role of substituent position played on OL performance of InPcCl, intensity transmittances of α-InPcCl and β-InPcCl are given in Fig. 3. It shows that both compounds exhibit outstanding nonlinear absorption properties while the OL performance of α-InPcCl is preferable. As shown in Fig. 3(a), transmittances of α-InPcCl and β-InPcCl decrease remarkably with the increase of input intensity, which is consistent with the experimental findings.[19] Molecules on the ground state S_0 are excited to the singlet excited state S_1 by absorbing the first photon, then part of the populations on S_1 state relaxes nonradiatively to the first triplet state T_1 through the fast intersystem crossing process (see Fig. 1(c)). Molecules in the excited states S_1 or T_1 will then absorb another photon to be promoted to the higher excited states S_n or T_2. In the case that the ESA cross section is larger than the GSA cross section, RSA will occur and the output intensity of the pulse will be strongly attenuated. Figure 3(b) displays the transmittance of pulse intensity as a function of the medium thickness with $I_0 = 4 \times 10^{12}$ W/m^2. It is obvious that the longer the propagation distance, the stronger the absorption. Interestingly, InPcCl with substituent at the α position has much lower transmittance than that with substituent at the β position owing to its faster intersystem crossing rate γ_c and larger photoabsorption cross section ratio of the lowest triplet state to the ground state (see Table 1). For laser dynamics in the nanosecond scale, the lifetime of the triplet state on the magnitude of microsecond is too long to be active, while the fast intersystem crossing plays a dominating role under this condition.

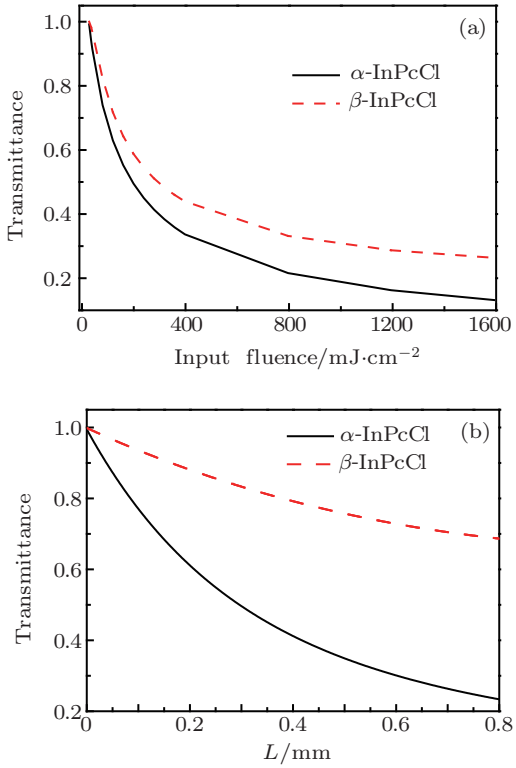


Fig. 3. (color online) Intensity transmittance (a) as a function of the peak intensity of the incident field through the absorbing medium ($z = 0.4$ mm) and (b) as a function of the thickness of the medium at $I_0 = 4 \times 10^{12}$ W/m^2 for α-InPcCl (solid line) and β-InPcCl (dashed line).

To visualize directly the OL performance of the two phthalocyanines, we present the output energy fluence of the field as a function of the input fluence at $z = 0.4$ mm in Fig. 4(a). The OL behavior is clearly demonstrated as expected and shows a good agreement with the experimental measurement in Ref. [19]. One can see that the output fluence increases slowly as the input fluence increases and becomes saturated after the OL threshold I_{th}, which is defined as the point at which the transmittance is half of the initial linear transmittance. The saturated transmittance of α-InPcCl is 46 percent smaller than that of β-InPcCl (0.14 for α-InPcCl and 0.26 for β-InPcCl at $z = 0.4$ mm with the initial fluence of 1600 mJ·cm^{-2}). Intuitively, the better OL performance of α-InPcCl may originate from α-InPcCl's larger concentration since the transmittance depends on both the propagation distance and the molecular concentration. To get rid of such confusion, different propagation distances for α-InPcCl and β-InPcCl are chosen in Fig. 4(b) by satisfying the condition that the products of propagation distances with concentrations are equal for α-InPcCl and β-InPcCl, namely, $N^{\alpha}_{cal} L^{\alpha} = N^{\beta}_{cal} L^{\beta}$. As shown in Fig. 4(b), with the same input fluence, the output fluence of α-InPcCl is still much smaller than that of β-InPcCl under the above condition, which indicates that the superior optical power limiting ability of α-InPcCl results from the inherent molecular attributes.

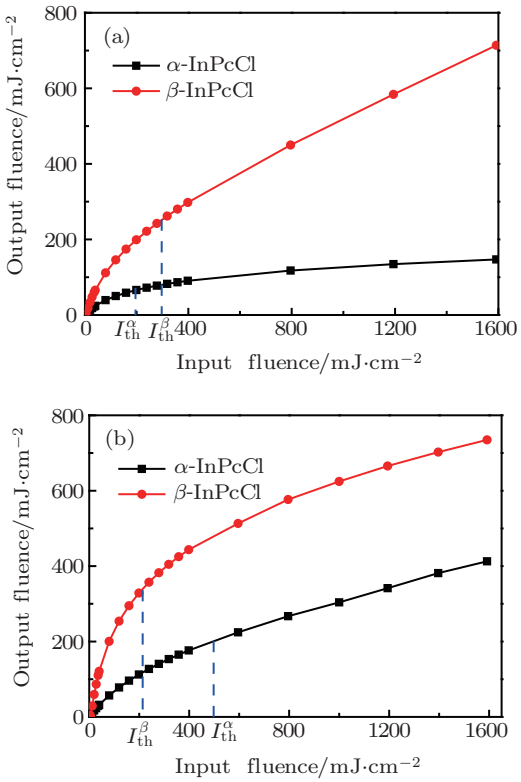


Fig. 4. (color online) Output fluence versus input fluence for α-InPcCl and β-InPcCl (a) at the same propagation distance of 0.4 mm and (b) at different propagation distances of 0.16 mm and 0.64 mm, respectively. $I_{\rm th}^{\alpha}$ and $I_{\rm th}^{\beta}$ are the OL thresholds for α-InPcCl and β-InPcCl, respectively.

Dynamics of population transfer for α-InPcCl on axis of the light beam without pulse propagation is shown in Fig. 5. At relatively low intensity $I_0 = 4 \times 10^{11}$ W/m^2 (Fig. 5(a)), population transfer mainly takes place in the ground state S_0 and the lowest triplet state T_1. The S_1 state is also slightly populated, indicating the contribution of the sequential channel $(S_0 \rightarrow S_1) \times (T_1 \rightarrow T_2)$ to be the main mechanism of nonlinear absorption. However, for a rather high intensity $I_0 = 4 \times 10^{12}$ W/m^2 (Fig. 5(b)), populations on the T_2 state are observable due to the excited triplet state absorption $T_1 \rightarrow T_2$. This can be verified from the obvious time delay δt relative to the ground state absorption $S_0 \rightarrow S_1$. One can also see from Fig. 5 that for a higher intensity, the response of the population transfer to the field is faster and the populations are saturated before the end of the pulse. Taking the radial distribution of the Gaussian pulse into consideration, figure 6 displays the transverse distribution of ρ_{S_0} and ρ_{T_1} near the entrance of the medium. When the light intensity is large enough, it transfers almost completely the population from the S_0 state to the T_1 state. The populations can be efficiently accumulated on the T_1 state, mainly benefiting from the fast intersystem crossing process and the long lifetime of the triplet state. The subfigures on the upper part of Fig. 6 show that the population transfer process occurs preferentially near the axis of the light beam where the field intensity is high and the effective transfer time is short (see Fig. 2).

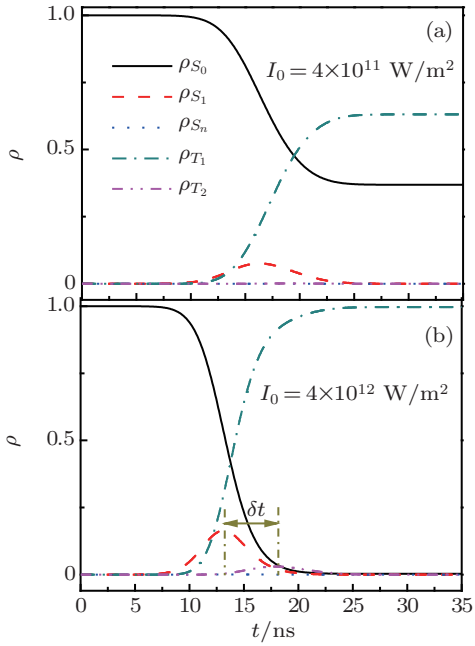


Fig. 5. (color online) Population evolutions of different states on the axis of the light beam ($r = 0$) without propagation of the pulse ($z = 0$). (a) $I_0 = 4 \times 10^{11}$ W/m^2, (b) $I_0 = 4 \times 10^{12}$ W/m^2.

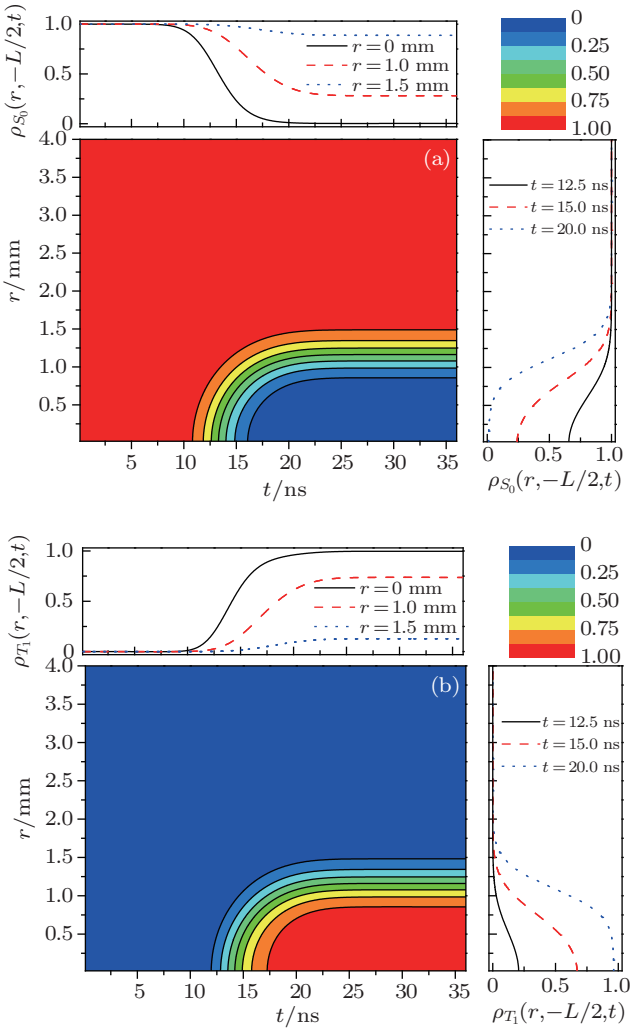


Fig. 6. (color online) Temporal and spatial evolutions of populations of (a) the ground and (b) the lowest triple states near the entrance of the medium. $I_0 = 4 \times 10^{12}$ W/m^2.

During pulse propagation, both transverse and longitudinal shapes of the Gaussian pulse will change dramatically on account of inhomogeneous photoabsorption and saturation effects. Figure 7 shows 2D maps of the output field intensity after passing through the absorbing medium of 0.8 mm long. One can see clearly that the rear part of the pulse is intensively attenuated and the shape of the pulse is strongly deformed during propagation, which is more severe in Fig. 7(b) for the incident field with higher intensity. The main reason is that for the front part of the pulse where the field intensity is weak, the linear GSA $S_0 \rightarrow S_1$ mainly occurs, while for the latter part of the pulse with higher field intensity, the state T_1 is fast populated by intersystem crossing process. Therefore, the sequential TPA $(S_0 \rightarrow S_1) \times (T_1 \rightarrow T_2)$ takes the dominating role and the pulse is drastically decreased. For the rear part of the pulse, although the field becomes weak, since the population has already been accumulated in the triplet state T_1, the field is still strongly absorbed due to the strong ESA $T_1 \rightarrow T_2$. These different absorption mechanisms of different parts of the pulse result in different radial distributions of the transmitted field.

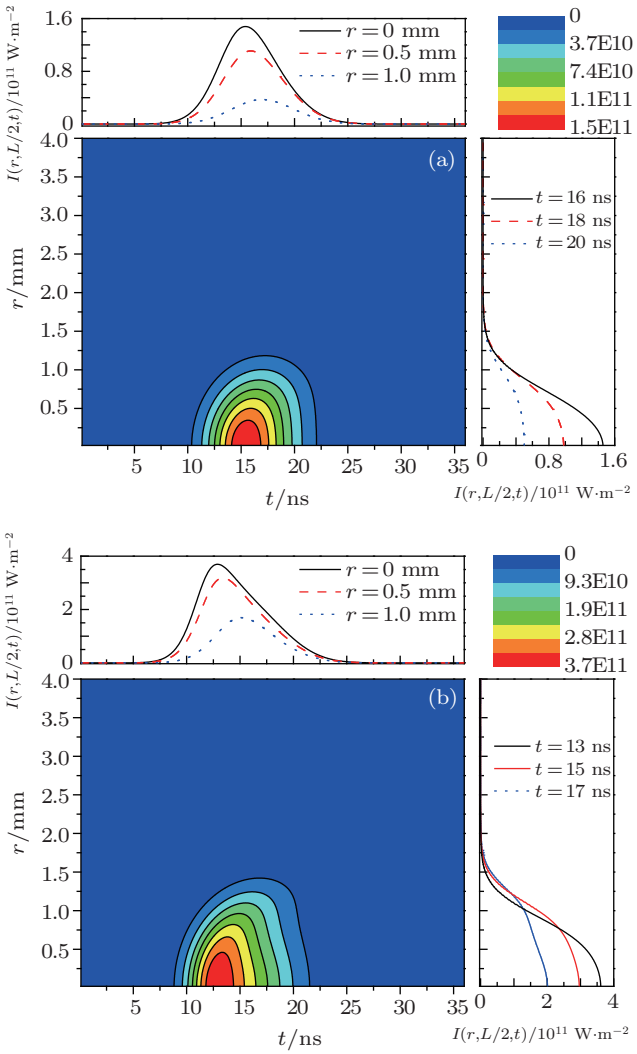


Fig. 7. (color online) Temporal and spatial evolutions of output field intensity after passing through the absorbing medium ($z = 0.4$ mm). (a) $I_0 = 4 \times 10^{11}$ W/m^2, (b) $I_0 = 4 \times 10^{12}$ W/m^2.

The strong nonlinear TPA $(S_0 \rightarrow S_1) \times (T_1 \rightarrow T_2)$ gives rise to the excellent OL behavior of the molecule. As we can see from Table 1, α-InPcCl has a higher triplet to singlet states ratio of the absorption cross sections, suggesting that it has better optical limiting performance. In order to get a more essential understanding of the physical mechanism, *ab-initio* calculations on the geometric and electronic structures of the compounds are employed. Figure 8 displays the highest occupied molecular orbitals (HOMO), the lowest unoccupied molecular orbitals (LUMO) and the charge variations between the charge transfer states and the ground states of α-InPcCl and β-InPcCl. In the aromatic macrocyclic plane of the molecules, the extent of the electron delocalization of α-InPcCl is much larger than that of β-InPcCl, which makes the intersystem crossing process of α-InPcCl easier to happen. Thus, α-InPcCl shows stronger optical absorption ability. Comparing the charge density differences of these two compounds, one can notice that the electrons transfer along the long axis of the α-InPcCl molecule while they transfer along the short axis in β-InPcCl, indicating that more electrons are transferred in α-InPcCl. As is known to all, frontier orbitals play a decisive role on the physical and chemical properties of molecules. Table 2 lists the energy differences ΔE between some frontier orbitals of α-InPcCl and β-InPcCl. It is noteworthy that values of α-InPcCl are smaller in comparison with those of β-InPcCl. When interacting with the external field, α-InPcCl is easier to excite, and thus more energy can be stored in the medium. Namely, it tends to possess stronger optical absorption ability.

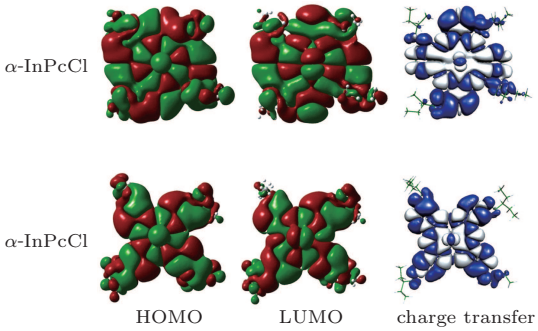


Fig. 8. (color online) HOMO, LUMO, and the charge variation (the white and blue areas represent the electron gain and loss, respectively) between the charge transfer states and the ground states of α-InPcCl and β-InPcCl.

Table 2. Energy differences between the frontier orbitals of α-InPcCl and β-InPcCl.

ΔE/(eV, HOMO-)	$\alpha-$InPcCl	$\beta-$InPcCl
LUMO	2.01691	2.09365
LUMO+1	2.04167	2.09501
LUMO+2	3.76551	3.88633
LUMO+3	4.11022	4.12797

4. Conclusions

The effect of substituent position on the OL properties of InPcCl is investigated by utilizing a five-level scheme to describe the medium and the two-dimensional paraxial wave equation to depict the field. Dynamics of population, which is characterized by the population transfer time between the ground state and the lowest triplet state, as well as evolution of the laser field, is presented. It is shown that substituent position has significant effect on the optical power limiting performance of the molecule. Our *ab-initio* calculations on the electronic structures of the compounds show that the phthalocyanine with α-substituent has extended electron delocalization and lower frontier orbital energy differences. This means that the phthalocyanine with substituent at the α-position has more active photophysical properties than that with substituent at the β-position, which is in good agreement with the experimental result. Our computational results provide a guideline for designing effective optical limiters.

References

[1] Lv Z W, Lv Y L and Yang J 2003 *Chin. Phys.* **12** 507

[2] Niu Y X, Yang H L, Zhang P, Shen X J, Jiang N, Chen Y and Tang F 2008 *Chin. Phys. B* **17** 3367

[3] Naseema K, Manjunatha K B, Sujith K V, Umesh G, Kalluraya B and Rao V 2012 *Opt. Mater.* **34** 1751

[4] Ma H, Leng J C, Liu M, Zhao L N and Jiao Y 2015 *Opt. Commun.* **350** 144

[5] Pritchett T M, Ferry M J, Mott A G, III W S, Haley J E, Liu R and Sun W F 2015 *Opt. Mater.* **39** 195

[6] Miao Q, Zhao P, Sun Y P, Liu J C and Wang C K 2008 *Acta Phys. Sin.* **58** 5455 (in Chinese)

[7] Thekkayil R, Philip R, Gopinath P and John H 2014 *Mater. Chem. Phys.* **146** 218

[8] Zhang Y J, Yang W J, Fan J Z, Song Y Z and Wang C K 2015 *Chin. J. Chem. Phys.* **28** 257

[9] Zhu P W, Wang P, Qiu W F, Liu Y Q and Ye C 2001 *Appl. Phys. Lett.* **78** 1319

[10] Rao S V, Anusha P T, Prashant T S, Swain D and Tewari S P 2011 *Mater. Sci. Appl.* **2** 299

[11] Yao C B, Zhang Y D, Chen D T, Yin H T, Yu C Q, Li J and Yuan P 2013 *Opt. Laser Technol.* **47** 228

[12] García-Frutos E M, Torre G d l, Vázquez P, Shirk J S and Torres T 2009 *Eur. J. Org. Chem.* **2009** 3212

[13] Wang A, Chen X L, Zhang L, Zhang G Y, Zhou L, Lu S, Zhou J H and Wei S H 2014 *J. Photoch. Photobio. A* **288** 1

[14] Łapok Ł, Cyza M, Gut A, Kępczyński M, Szewczyk G, Sarna T and Nowakowska M 2014 *J. Photoch. Photobio. A* **286** 55

[15] Chen J, Gan Q, Li S Y, Gong F B, Wang Q, Yang Z P, QingWang S, Xu H, Ma J S and Yang G Q 2009 *J. Photoch. Photobio. A: Chem.* **207** 58

[16] Liu Y, Chen Y, Cai L Z, Wang J, Lin Y, Doyle J J and Blau W J 2008 *Mater. Chem. Phys.* **107** 189

[17] Nyokong T 2007 *Coordin. Chem. Rev.* **251** 1707

[18] Snow A W, Shirk J S and Pong R G S 2001 *J. Porphy. Phthalocya.* **05** 582

[19] Wang S Q, Gan Q, Zhang Y F, Li S Y, Xu H J and Yang G Q 2006 *Chem. Phys. Chem* **7** 935

[20] Gavrilyuk S, Liu J C, Kamada K, Ågren H and Gel'mukhanov F 2009 *J. Chem. Phys.* **130** 054114

[21] Wang C K, Zhao P, Miao Q, Sun Y P and Zhou Y 2010 *J. Phys. B: At. Mol. Opt. Phys.* **43** 105601

[22] Miao Q, Ding H J, Sun Y P, Gel'mukhanov F and Wang C K 2012 *J. Phys. B: At. Mol. Opt. Phys.* **45** 085402

[23] Gaussian 09